



Available online at [www.sciencedirect.com](http://www.sciencedirect.com)



ScienceDirect

Trans. Nonferrous Met. Soc. China 27(2017) 2400–2405

Transactions of  
Nonferrous Metals  
Society of China

[www.tnmsc.cn](http://www.tnmsc.cn)



## Effect of carbon on high temperature compressive and creep properties of $\beta$ -stabilized TiAl alloy

Can-xu ZHOU, Bin LIU, Yong LIU, Cong-zhang QIU, Hui-zhong LI, Yue-hui HE

State Key Laboratory of Powder Metallurgy, Central South University, Changsha 410083, China

Received 23 February 2017; accepted 21 June 2017

**Abstract:** Carbon is an important alloying element in improving high temperature mechanical properties of various metallic materials. The effects of carbon on high temperature mechanical properties of a  $\beta$ -stabilized Ti–45Al–3Fe–2Mo (molar fraction, %) alloy were studied through compressive and creep tests. The results show that the carbon addition (0.5%, molar fraction) obviously enhances the high temperature compressive strength and creep resistance of the  $\beta$ -stabilized Ti–45Al–3Fe–2Mo alloy. A lot of nano-scaled  $Ti_3AlC$  carbides precipitate in the  $\beta$ -stabilized alloy and these carbides pin the dislocations, and greatly increase the high temperature properties. At the same time, the carbon addition decreases the amount of  $\beta$  phase, refines the lamellar spacing, and causes solution strengthening, which also contribute to the improvement of the high temperature properties.

**Key words:** TiAl alloy; carbon; precipitation; high temperature compression; high temperature creep

### 1 Introduction

TiAl-based alloys possess low density, high strength and good oxidation resistance, which make them excellent candidates for high temperature applications [1–3]. Depended on the improvement of alloy chemistry and microstructure, TiAl alloys have already been found application in automotive and aircraft engine industries; however, more efforts are still needed to improve the workability of TiAl. One way to increase the high temperature plasticity of TiAl alloys is to add alloying elements to form  $\beta$  phase at elevated temperatures [4]. More and more TiAl alloys based on the  $\beta$ -TiAl phase have been found application in aerospace and automotive industries [5,6]. The disordered  $\beta$  phase with a bcc lattice structure provides a sufficient number of independent slip systems, and is softer than  $\alpha_2$  and  $\gamma$  phases, so that  $\beta$  phase-contained TiAl alloys could be hot forged under near conventional condition. A number of studies have demonstrated that  $\beta$  phase can be stabilized through alloying with either  $\beta$ -isomorphous elements, such as Nb, V, and Ta, or  $\beta$ -eutectoid elements, such as Cr, Fe, Mn, Ni and W [7–10]. In our previous works [11–13], a

Ti–45Al–3Fe–2Mo alloy ( $\beta$ -TiAl) has been designed, which has a nearly full lamellar microstructure, with  $\beta$  and  $\gamma$  phases coexisting along the grain boundaries. The alloy shows outstanding high temperature deformability originating from the dynamic recrystallization occurred in  $\beta$  grains at elevated temperatures. However, the introduction of the  $\beta$  phase may deteriorate the compression strength and creep resistance at elevated temperatures. One way to solve this dilemma is to eliminate the  $\beta$  phase by subsequent heat treatments after hot working [14], but it is usually difficult since  $\beta$  phase usually contains stabilizing elements of high melting points. The addition of interstitial elements, such as carbon, is another way to increase the high temperature properties of TiAl alloys. A plenty of works have demonstrated that the addition of carbon can improve the creep resistance of  $\gamma$ -TiAl alloys [15–17]. However, for the  $\beta$ -stabilized TiAl alloys, the effect of carbon on the high temperature properties remains unclear.

In the present work, the effects of carbon addition on the high temperature compressive strength and creep resistance of the  $\beta$ -stabilized Ti–45Al–3Fe–2Mo alloy were studied, and the intrinsic mechanisms were also discussed.

**Foundation item:** Project (2014CB664402) supported by the National Basic Research Program of China; Project (2016YFB0700302) supported by the National Major Scientific Research Development Program, China; Project (2017JJ2311) supported by the Hunan Natural Science Foundation of China

**Corresponding author:** Bin LIU; Tel: +86-731-88877669; E-mail: binliu@csu.edu.cn  
DOI: 10.1016/S1003-6326(17)60266-8

60% of methanol (volume fraction) at  $-30^{\circ}\text{C}$  and 20 V.

## 2 Experimental

A  $\beta$ -stabilized TiAl based alloys with compositions of Ti–45Al–3Fe–2Mo–xC ( $x=0, 0.5$ , molar fraction, %) were prepared by a vacuum arc melting method. To ensure compositional uniformity, the alloys were remelted at least 4 times. The ingots were then homogenized at  $1200^{\circ}\text{C}$  for 24 h and  $900^{\circ}\text{C}$  for 2 h, followed by air cooling. Samples for hot compression and creep tests were machined from the homogenized ingots. The compression samples have a diameter of 8 mm and a height of 12 mm, and the creep test samples have a diameter of 6 mm and a length of 30 mm in the gauge area. Compression tests were conducted at  $750\text{--}850^{\circ}\text{C}$  and strain rate of  $1\times 10^{-4}\text{ s}^{-1}$  on an Instron 3369 machine. Creep tests were carried out at  $750^{\circ}\text{C}$  for 300 h under a constant loading of 100–300 MPa on a MTS-GWT 2105 machine. The microstructures of the samples before and after deformation were observed by using an field emission scanning electron microscope (FE-SEM, FEI NOVA NANOSEM 230) and transmission electron microscope (TEM, JEOL 2100F). The specimens for SEM observation were electrolytically polished by using 30 mL nitric acid and 70 mL methanol solution, and the TEM specimens were prepared by twin jet-polishing in an electrolyte solution containing 5% of perchloric acid, 35% of butanol and

## 3 Results

### 3.1 Initial microstructures

Figure 1 shows the microstructures of the Ti–45Al–3Fe–2Mo–xC alloys before hot compressive and creep tests. The Ti–45Al–3Fe–2Mo alloy and Ti–45Al–3Fe–2Mo–0.5C alloy both consist of  $\alpha_2/\gamma$  lamellar colonies,  $\gamma$  phase and  $\beta$  phase. The average colony size, lamellar spacing and volume fraction of the  $\beta$  phase of the C-free alloy are 24.2  $\mu\text{m}$ , 267 nm and 15.4%, respectively; those values for the C-doped alloy are 52.6  $\mu\text{m}$ , 155 nm and 9.7%, respectively. Therefore, the addition of carbon has great influence on the microstructure of the  $\beta$ -stabilized TiAl alloy, i.e., increasing the colony size, refining the lamellar spacing, and decreasing the amount of  $\beta$  phase.

### 3.2 High temperature compressive property

Figure 2 shows the flow curves of the Ti–45Al–3Fe–2Mo–xC alloys deformed at temperatures ranging in  $750\text{--}850^{\circ}\text{C}$  and a strain rate of  $1\times 10^{-4}\text{ s}^{-1}$ . It is shown that the carbon addition improves the high temperature compressive strength of the  $\beta$ -stabilized TiAl alloy. The peak stresses of the C-free alloy at 750, 800 and  $850^{\circ}\text{C}$  are 438, 352 and 245 MPa, respectively, while the peak stresses for the C-doped alloy increase to

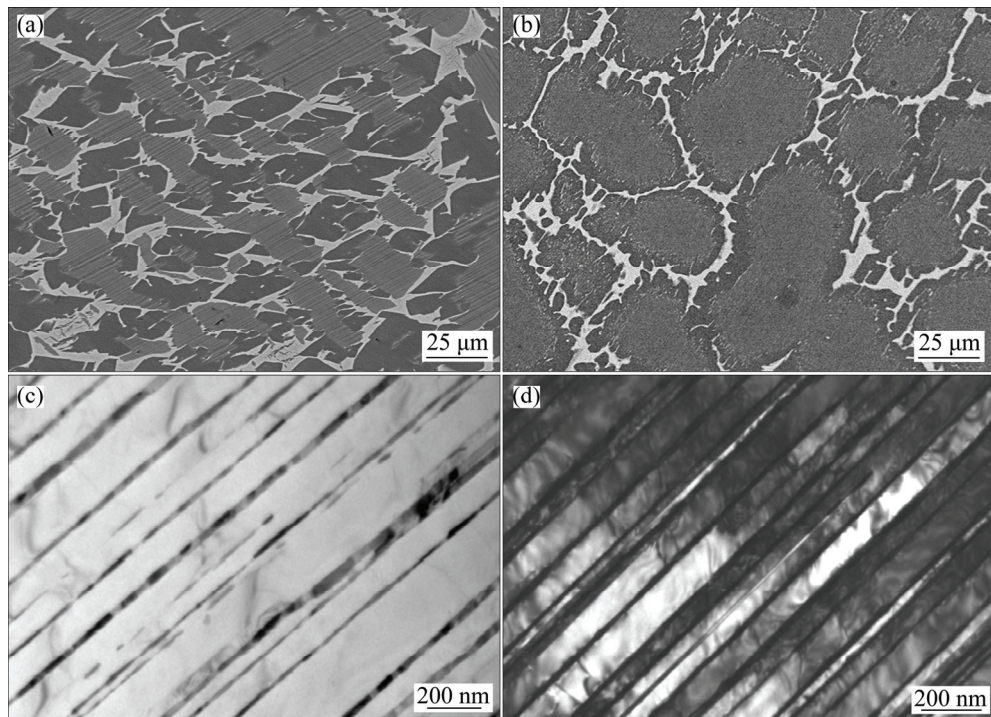


**Fig. 1** SEM images (BSE mode) (a, b) and TEM bright field images (c, d) of Ti–45Al–3Fe–2Mo–xC alloys: (a, c) Ti–45Al–3Fe–2Mo; (b, d) Ti–45Al–3Fe–2Mo–0.5C (White phase, grey phase and dark phase in (a) and (b) correspond to  $\beta$ ,  $\alpha_2$  and  $\gamma$  phase, respectively)

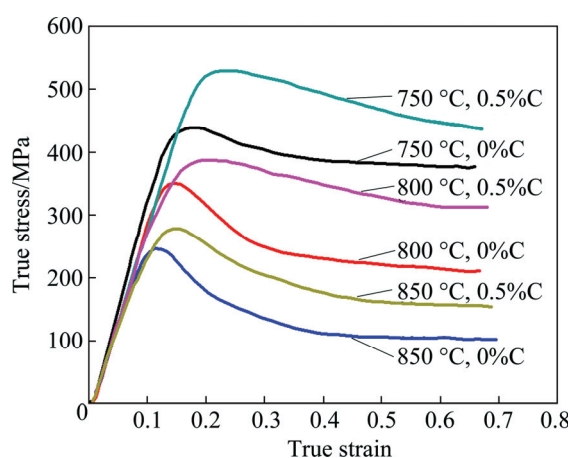


**Fig. 2** Compressive flow curves of Ti-45Al-3Fe-2Mo-xC alloys deformed at 750–850 °C with strain rate of  $10^{-4} \text{ s}^{-1}$

about 530, 395 and 275 MPa under the same condition. The high temperature compressive strength is closely related to the microstructures. The decrease in the volume fraction of  $\beta$  phase significantly reduces the deformability and increases the high temperature strength because the bcc  $\beta$  phase is a soft phase at the

testing temperatures. At the same time, the reducing of the lamellar spacing restrains the dislocation movement, and increases the high temperature compressive strength correspondingly. Therefore, the C-doped alloys show less flow-softening characteristics compared with the C-free alloy.

Figure 3 shows the SEM images of the Ti-45Al-3Fe-2Mo-xC alloys deformed at 800 °C to a strain of 0.5. In both alloys, the lamellar colonies become kinked, and a large amount of fine grains induced by dynamic recrystallization can be observed in the grain boundary  $\beta$  phases. Figure 4 shows the TEM images of the Ti-45Al-3Fe-2Mo-0.5C alloy deformed at 800 °C. A large number of nano-scaled precipitates in a size of 10–20 nm can be observed, and strong entanglement of dislocations with particles can be seen. SAED results show that the precipitates are  $\text{Ti}_3\text{AlC}$  carbides, and the orientation relationship between the carbide and  $\gamma$ -TiAl phase can be determined as  $(001)_p//(001)_\gamma$  and  $[010]_p//[010]_\gamma$ . This indicates that the  $\text{Ti}_3\text{AlC}$  precipitates pin the dislocations (Fig. 4(a)), restrain the movement of dislocation, and thus, greatly increase the high temperature strength.

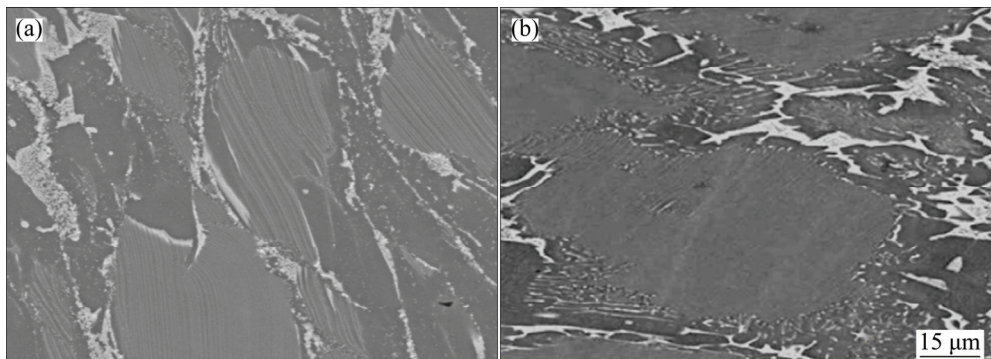


**Fig. 3** SEM images (BSE mode) of Ti-45Al-3Fe-2Mo (a) and Ti-45Al-3Fe-2Mo-0.5C (b) alloys deformed at 800 °C with strain rate of  $10^{-4} \text{ s}^{-1}$

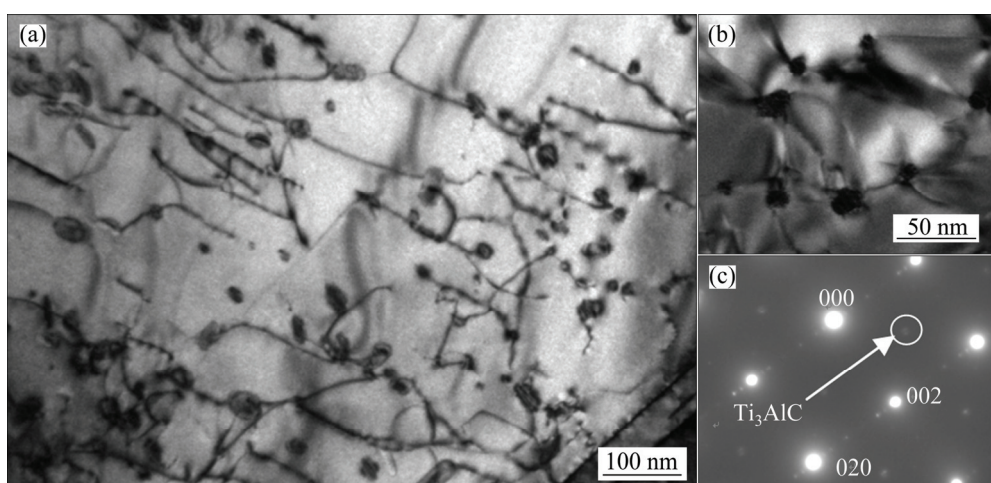


**Fig. 4** TEM images of Ti-45Al-3Fe-2Mo-0.5C alloy compressed at 800 °C with strain rate of  $10^{-4} \text{ s}^{-1}$ : (a) Dislocation structure; (b) Interaction between  $\text{Ti}_3\text{AlC}$  particles and dislocations; (c) SAED pattern

### 3.3 Elevated temperature creep property

Figure 5 shows the strain–time curves of the Ti–45Al–3Fe–2Mo–xC alloys tested at temperature of 750 °C with applied stress of 150–300 MPa. It is clear that the creep strains for the C-doped alloy are much lower than those of the C-free alloy under the same condition. For example, at  $8 \times 10^5$  s, the creep strain under 200 MPa for the C-doped alloy is about 2.65%, which is about 60% lower than that of the C-free alloy. This result suggests that the C-doped alloy possesses better creep resistance than the C-free alloy. Figure 6 shows the relationship between the minimum creep rate and the effective stress for the Ti–45Al–3Fe–2Mo–xC alloys. The stress exponent  $n$  can be deduced from the slope of the lines. The  $n$  value of the C-free alloy is about 2.05, which suggests that the creep deformation is controlled by the grain boundary sliding. The value of  $n$  for the C-doped alloy is about 3.3. A high stress exponent of the C-doped alloy suggests the retarding effect of the precipitates on the dislocation movement. Figure 7 shows the TEM images of the Ti–45Al–3Fe–2Mo–xC alloys after the creep test at 750 °C and 200 MPa. For the C-free alloy, dislocation piles up at the boundaries

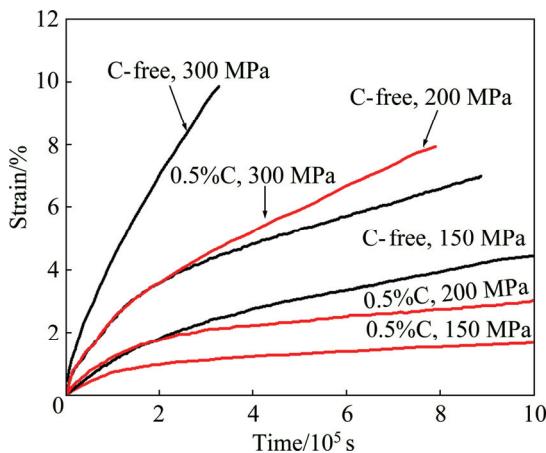


**Fig. 5** Creep curves of Ti–45Al–3Fe–2Mo–xC alloys with testing temperature of 750 °C

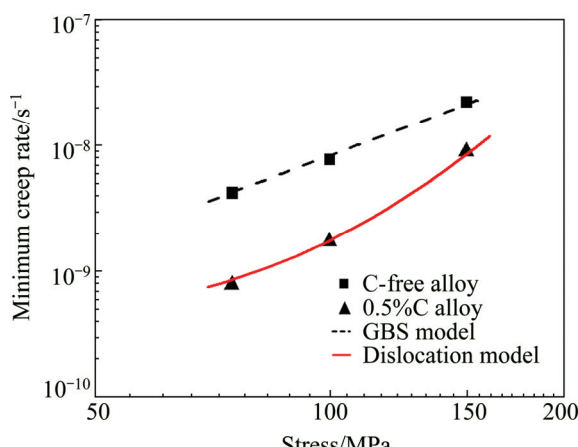


**Fig. 6** Minimum creep rate as function of applied stress

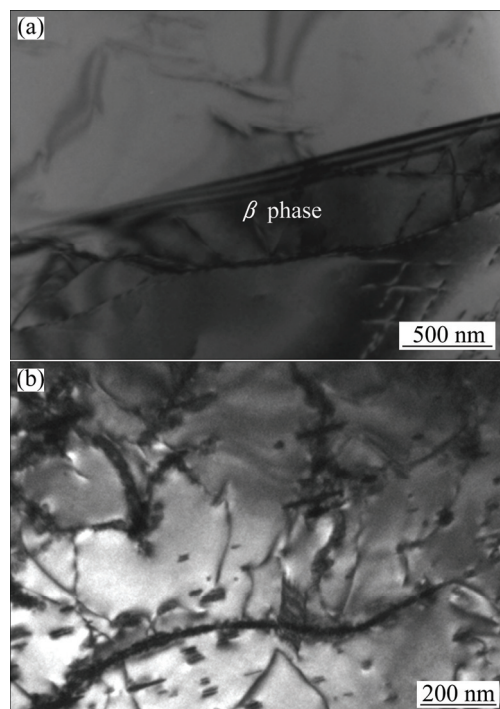


**Fig. 7** TEM images of Ti–45Al–3Fe–2Mo–xC alloys after creep at 750 °C and 200 MPa: (a) Ti–45Al–3Fe–2Mo alloy; (b) Ti–45Al–3Fe–2Mo–0.5C alloy

between the lamellar colony and  $\beta$  grains. However, for the C-doped alloy, the precipitation of nano-sized carbides can be found in the  $\gamma$  matrix. The dislocations are pinned and tangled together around the fine precipitates. Figure 8 shows the STEM image and the compositional mappings of Ti–45Al–3Fe–2Mo–0.5C alloy after the creep deformation at 750 °C and 200 MPa. Some particles with particle size of about 30–50 nm precipitate at the  $\alpha_2/\gamma$  interfaces. The particles contain a high content of carbon and titanium, which is in accordance with the SAED result in Fig. 4.

## 4 Discussion

For the  $\beta$ -stabilized Ti–45Al–3Fe–2Mo alloy, the Nb equivalent value can be calculated to be 32% according to the equation of  $[Nb] = Nb + 8/3(Cr + Mn) + 8/5V + 4(W + Mo) + 8Fe$  [18], which is much higher than 9.5%, therefore, the solidification pathway is  $L \rightarrow L + \beta \rightarrow \beta \rightarrow \beta + \alpha \rightarrow (\beta + \gamma) + \text{lamellar } (\alpha_2 + \gamma)$ . The  $\beta$  phase exists during the whole solidification process, which can restrain the growth of  $\alpha$  grain. Carbon is an  $\alpha$ -stabilized element, and is supposed to increase the amount of  $\alpha$  phase and reduce the amount of retained  $\beta$  phase, thus it can weaken the refining effect of  $\beta$  phase on microstructure and increase the colony size. During the transformation from  $\alpha$  to  $\alpha_2/\gamma$ , the growth of the laths usually occurs through the “terrace–ledge–kink” mechanism [19]. Atoms are transferred into kinks which

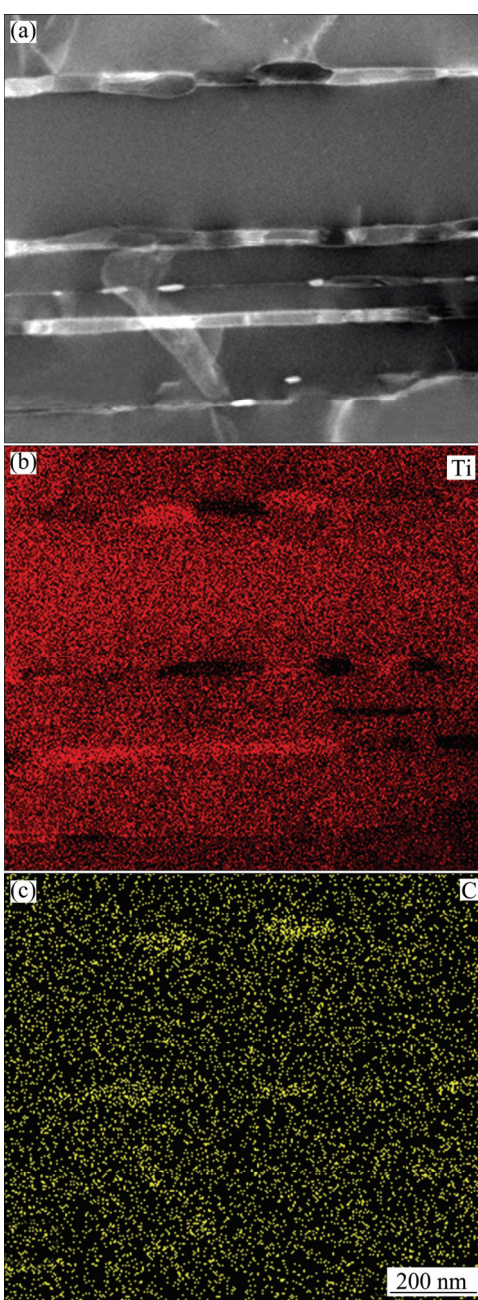


**Fig. 8** STEM image (a) and compositional mappings (b, c) of  $\beta$ -stabilized Ti–45Al–3Fe–2Mo–0.5C alloy after creep at 750 °C and 200 MPa

provide favorable sites. The solute carbon atoms enhance the heterogeneous nucleation rate by reducing the stacking fault energy, and decrease the thickening rate of lamellar by retarding lateral jumps of atoms across the lamellar interface [20]. Meanwhile, the precipitation of carbides on the  $\alpha_2/\gamma$  interface can hinder the growth of both  $\alpha_2$  and  $\gamma$  laths. These effects cause the decremental of  $\alpha_2/\gamma$  lamellar spacing. In general, the addition of carbon reduces the amount of  $\beta$  phase, refines the lamellar spacing, and precipitates the nano-sized carbides, which leads to the improvement of high temperature properties. In addition, solid solution of

carbon can also improve the elevated mechanical property of the present  $\beta$ -stabilized TiAl alloy because the carbon atoms are glide obstacles for dislocations, which cannot be overcome completely with the aid of thermal activation.

For a steady creep, there is a balance between the generation rate and the annihilation rate of dislocations. The creep rate is related with the value of the stress exponent  $n$ . In general, the  $n$  values are usually in the range of 2–7 for pure metals, ceramics and many alloys over a relatively wide range of temperatures and strain rates [21]. Different values of  $n$  correspond to different creep mechanisms, i.e. high stress exponents ( $>3.2$ ) are related to dislocation climb, while low  $n$  values are owing to the grain boundary sliding (GBS) [22]. For the C-free alloy, the value of  $n$  is nearly 2.05, therefore, GBS process is expected to occur during the creep deformation. The minimum creep rate for GBS-controlled deformation of TiAl alloys has been developed in Ref. [23] as follows:

$$\dot{\varepsilon}_{\min} = D_{gb0} \exp\left(\frac{-218000}{RT}\right) d^{-2} \sigma^2 \quad (1)$$

where  $D_{gb0}$  is the grain boundary diffusion coefficient,  $d$  is the grain size,  $\sigma$  is the applied stress,  $R$  is the gas constant, and  $T$  is the absolute temperature. The  $D_{gb0}$  can be determined to be  $75 \text{ } \mu\text{m}^2 \cdot \text{s}^{-1} \cdot \text{MPa}^{-2}$  by fitting the experiment data, therefore, the minimum creep rate for the C-free alloy is about  $2.2 \times 10^{-8} \text{ s}^{-1}$ . It is noted that the  $D_{gb0}$  is higher than that of the ordinary TiAl alloy ( $D_{gb0} = 63.4 \text{ } \mu\text{m}^2 \cdot \text{s}^{-1} \cdot \text{MPa}^{-2}$ ), which is caused by the existence of the  $\beta$  phase. The  $\beta$  phase is a soft phase at high temperatures [24], and it is expected to act like a lubricant and favoring GBS process, as shown in Fig. 7(a).

For the C-doped alloy, the colony size increases to about  $52.6 \text{ } \mu\text{m}$ , and the value of  $n$  increases to 3.4. The high value of  $n$  and the low volume fraction of  $\beta$  phase (Fig. 1) suggest that the dislocation-gliding mechanism may work for the increased creep resistance. The model for the mechanism of the dislocation gliding [23] can be used to describe the creep process of the C-doped alloy:

$$\dot{\varepsilon}_{\min} = K_0 \exp\left(\frac{-375000}{RT}\right) \sinh\left(\frac{\sigma}{\sigma_0}\right) \quad (2)$$

where  $\sigma$  is the applied stress,  $\sigma_0$  is material and temperature dependent constant, and constant  $K_0$  is related to  $Q$ . In the present work,  $\sigma_0$  and  $K_0$  are determined as 28 MPa and  $2.3 \times 10^9 \text{ s}^{-1}$  through fitting the experimental data. Therefore, the minimum creep rate for the C-doped alloy can be determined to be about  $7.9 \times 10^{-9} \text{ s}^{-1}$ . This value is about 1/3 that of the C-free alloy, suggesting the improvement of the creep resistance.

## 5 Conclusions

1) For the  $\beta$ -stabilized Ti-45Al-3Fe-2Mo alloy, the carbon addition increases the  $\alpha_2/\gamma$  colony size, refines the lamellar spacing, deceases the amount of  $\beta$  phase and induces the precipitation of  $Ti_3AlC$  particles.

2) The carbon addition obviously improves the high temperature compressive strength and creep resistance of the  $\beta$ -stabilized Ti-45Al-3Fe-2Mo alloy.

3) The improvement of high temperature properties is believed to be caused by the precipitation strengthening of the  $Ti_3AlC$  particles, the refinement of the lamellar microstructure, the reducing of the amount of  $\beta$  phase and the solution strengthening of the interstitial carbon elements.

## References

- [1] KOTHARI K, RADHAKRISHNAN R, WERELEY N M. Advances in gamma titanium aluminides and their manufacturing techniques [J]. Progress in Aerospace Sciences, 2012, 55: 1–16.
- [2] KIM Y W, DIMIDUK D M. Strain-rate effects on the room temperature tensile properties of a TiAl alloy [J]. MRS Online Proceedings Library, 1992, 288: 671–678.
- [3] SUN Hong-fei, LI Xue-wen, FANG Wen-bin. Microstructures of PM Ti-45Al-10Nb alloy fabricated by reactive sintering [J]. Transactions of Nonferrous Metals Society of China, 2015, 25(5): 1454–1459.
- [4] KASTENHUBER M, RASHKOVA B, CLEMENS H, MAYER S. Enhancement of creep properties and microstructural stability of intermetallic  $\beta$ -solidifying  $\gamma$ -TiAl based alloys [J]. Intermetallics, 2015, 63: 19–26.
- [5] IMAYEV R M, IMAYEV V M, OEHRING M, APPEL F. Alloy design concepts for refined gamma titanium aluminide based alloys [J]. Intermetallics, 2007, 15: 451–460.
- [6] JIANG Hai-tao, ZENG Shang-wu, ZHAO Ai-min, DING Xiao-nan, DONG Peng. Hot deformation behavior of  $\beta$  phase containing  $\gamma$ -TiAl alloy [J]. Materials Science and Engineering A, 2016, 661: 160–167.
- [7] HUANG Lan, LIAW P K, LIU C T, LIU Yong, HUANG Jin-song. Microstructural evolution of (TiAl)+Nb+W+B alloy [J]. Transactions of Nonferrous Metals Society of China, 2011, 21(10): 2192–2198.
- [8] BEDDOES J, CHEN W R, ZHAO L. Precipitation of  $\beta$  particles in a fully lamellar Ti-47Al-2Nb-1Mn-0.5W-0.5Mo-0.2Si (at.%) alloy [J]. Journal of Materials Science, 2002, 37: 621–627.
- [9] NIU H Z, CHEN Y Y, XIAO S L, XU L J. Microstructure evolution and mechanical properties of a novel beta  $\gamma$ -TiAl alloy [J]. Intermetallics, 2012, 31: 225–231.
- [10] TAKEYAMA M, OHMURA Y, KIKUCHI M, MATSUO T. Phase equilibria and microstructural control of gamma TiAl based alloys [J]. Intermetallics, 1998, 8: 643–646.
- [11] QIU Cong-zhang, LIU Yong, HUANG Lan, ZHANG Wei, LIU Bin, LU Bin. Effect of Fe and Mo additions on microstructure and mechanical properties of TiAl intermetallics [J]. Transactions of Nonferrous Metals Society of China, 2012, 22(3): 521–527.
- [12] QIU Cong-zhang, LIU Yong, ZHANG Wei, LIU Bin, LIANG Xiao-peng. Development of a Nb-free TiAl-based intermetallics with a low-temperature superplasticity [J]. Intermetallics, 2012, 27: 46–51.
- [13] ZHOU Can-xu, ZENG F P, LIU Bin, LIU Yong, ZHAO Kun, LU Jin-zhong, QIU Cong-zhang, LI Jian-bo, HE Yue-hui. Effects of Si on microstructures and high temperature properties of beta stabilized TiAl alloy [J]. Materials Transactions, 2016, 57: 461–465.
- [14] ZHU Han-liang, SEO D Y, MARUYAMA K. Strengthening behavior of beta phase in lamellar microstructure of TiAl alloys [J]. JOM, 2010, 62: 66–69.
- [15] IMAYEV R M, IMAYEV V M, KHISMATULLIN T G, OEHRING M, APPEL F. The physics of metals and metallography [J]. The Physics of Metals and Metallography, 2006, 102: 105–113.
- [16] APPEL F, OEHRING M, WAGNER R. Novel design concepts for gamma-base titanium aluminide alloys [J]. Intermetallics, 2000, 8: 1283–1312.
- [17] CLEMENS H, MAYER S. Design, processing, microstructure, properties, and applications of advanced intermetallic TiAl alloy [J]. Advanced Engineering Materials, 2013, 15: 191–215.
- [18] DONG Shu-lin, CHEN Rui-run, GUO Jing-jie, DING Hong-sheng, SU Yan-qing, FU Heng-zhi. Microstructure and room temperature tensile property of as-cast Ti-44Al-6Nb-1.0Cr-2.0V alloy [J]. Transactions of Nonferrous Metals Society of China, 2015, 25(4): 1097–1105.
- [19] DENQUIN A, NAKA S. Phase transformation mechanisms involved in two-phase TiAl-based alloys—I. Lamellar structure formation [J]. Acta Mater, 1996, 44: 343–352.
- [20] PARK H S, NAM S W, KIM N J, HWANG S K. Refinement of the lamellar structure in TiAl-based intermetallic compound by addition of carbon [J]. Scripta Mater, 1999, 41: 1197–1203.
- [21] KASSNER. Fundamentals of creep in metals and alloys [M]. Weinheim: Wiley-VCH, 2004.
- [22] APPEL F. Gamma titanium aluminide alloys [M]. Weinheim: Wiley-VCH, 2011.
- [23] ZHANG W J, DEEVI S C. Analysis of the minimum creep rates of TiAl alloys [J]. Materials Science and Engineering A, 2003, 362: 280–291.
- [24] WANG J G, NIEH T G. Creep of a beta phase-containing TiAl alloy [J]. Intermetallics, 2000, 8: 737–748.

## 元素 C 对 $\beta$ -TiAl 合金高温压缩及蠕变性能的影响

周灿旭, 刘彬, 刘咏, 邱从章, 李慧中, 贺跃辉

中南大学 粉末冶金国家重点实验室, 长沙 410083

**摘要:** C 元素是提高金属材料高温性能的重要元素之一。研究 C 元素对  $\beta$ -TiAl 合金(Ti-45Al-3Fe-2Mo, 摩尔分数, %)的高温压缩性能( $750\sim850^{\circ}\text{C}$ )及蠕变性能( $750^{\circ}\text{C}$ ,  $150\sim300\text{ MPa}$ )的影响。结果表明, C 元素的加入明显提高  $\beta$ -TiAl 合金的高温压缩强度及蠕变抗力。添加 C 元素后, 在  $\beta$ -TiAl 合金中形成了纳米尺度的  $Ti_3AlC$  碳化物相, 碳化物可以钉扎位错, 从而大幅提高材料的高温性能。同时, C 元素的添加还降低  $\beta$  相含量, 细化层片结构, 引起固溶强化, 这些因素的共同作用都有效提高合金的高温性能。

**关键词:** TiAl 合金; 碳; 析出; 高温压缩; 高温蠕变

(Edited by Bing YANG)